Supporting Information: Origin of the Anomalous Electronic Shot Noise in Atomic-Scale Junctions

Anqi Mu,[a†] Ofir Shein-Lumbroso[a],[‡] Oren Tal,[‡] and Dvira Segal[*,†]

†*Department of Chemistry and Centre for Quantum Information and Quantum Control, University of Toronto, 80 Saint George St., Toronto, Ontario, Canada M5S 3H6*

‡*Department of Chemical and Biological Physics, Weizmann Institute of Science, Rehovot, Israel*

E-mail: dvira.segal@utoronto.ca

[a]A.M. and O.S.L. contributed equally to this work

S1 Working formulae

To make our analysis self-contained, in this Section we describe our modeling and theoretical expressions. This information is partially included in the Method section of the main text, but we repeat it here for completeness. We consider coherent, elastic transport of electrons in a two-terminal junction. The metals include collections of noninteracting electrons with occupation numbers following the grand canonical ensemble; the Fermi function $f(\epsilon, \mu_\nu, T) = \frac{1}{e^{\beta(\epsilon-\mu_\nu)}+1}$ is evaluated at the chemical potential μ_ν and temperature T with the inverse temperature $\beta = 1/k_B T$; $\nu = L, R$. Below we denote by μ the equilibrium Fermi energy. Ignoring decoherence and inelastic processes within the constriction, the average current is given by the Landauer formula,

$$\langle I \rangle = \frac{2e}{h} \int_{-\infty}^{\infty} d\epsilon \tau(\epsilon) \left[f(\epsilon, \mu_L, T) - f(\epsilon, \mu_R, T) \right]. \tag{S1}$$

The corresponding zero frequency power spectrum of the noise is given by [1]

$$\begin{aligned} S &= S_1 + S_2 \\ S_1 &= \frac{4e^2}{h} \int_{-\infty}^{\infty} d\epsilon \{ f(\epsilon, \mu_L, T)[1 - f(\epsilon, \mu_L, T)] + f(\epsilon, \mu_R, T)[1 - f(\epsilon, \mu_R, T)] \} \tau^2(\epsilon), \\ S_2 &= \frac{4e^2}{h} \int_{-\infty}^{\infty} d\epsilon \{ f(\epsilon, \mu_R, T)[1 - f(\epsilon, \mu_L, T)] + f(\epsilon, \mu_L, T)[1 - f(\epsilon, \mu_R, T)] \} \tau(\epsilon)[1 - \tau(\epsilon)]. \end{aligned} \tag{S2}$$

In this partition of the total noise, S_1 includes additive terms in the left and right metals while S_2 collects transport processes from one terminal to the other. The transmission function $\tau(\epsilon)$ is energy dependent; voltage and temperature dependency, rooted in many-body effects, are sometimes phenomenologically introduced into the transmission function—though not in our work.

To derive the standard result for the shot noise, one assumes a constant transmission function. In this work, we write down a Taylor expansion for the transmission function,

performed around the equilibrium Fermi energy μ,

$$\tau(\epsilon) \approx \tau(\mu) + \left.\frac{d\tau}{d\epsilon}\right|_{\mu} (\epsilon - \mu). \tag{S3}$$

For simplicity, we denote $\tau(\mu)$ by τ_0 and $\tau'(\mu) \equiv \left.\frac{d\tau}{d\epsilon}\right|_{\mu}$. Another central ingredient of our work is that we allow the applied potential to drop asymmetrically around the equilibrium Fermi energy,

$$\begin{aligned} \mu_L &= \mu + \alpha\Delta\mu, \\ \mu_R &= \mu - (1-\alpha)\Delta\mu, \end{aligned} \tag{S4}$$

with $0 \leq \alpha \leq 1$; when $\alpha = 1/2$, the potential bias is partitioned symmetrically at the two ends.

S2 Review of "normal shot noise": Constant transmission function

Let us now review the standard, 'normal' shot noise expression, which is used to fit experimental observations of shot noise at low voltage. Equations (S1)-(S2) can be simplified if $\tau(\epsilon)$ is assumed a constant. This assumption is justified at low bias voltage. Then, e.g., the width of resonances (responsible for charge transport through the conductor) is considerable relative to the bias window and the transmission function can be approximated by its (fixed) value at the Fermi energy. Making this critical assumption, the averaged current under a finite voltage reduces to $\langle I \rangle = \frac{2e}{h}\Delta\mu \sum_i \tau_{0,i}$, with the power noise[1,2]

$$\begin{aligned} S^T_{\Delta\mu} &= 4k_BTG_0 \sum_i \tau_{0,i}^2 \\ &+ 2\Delta\mu \coth\left(\frac{\Delta\mu}{2k_BT}\right) G_0 \sum_i \tau_{0,i}(1-\tau_{0,i}). \end{aligned} \tag{S5}$$

Here $\Delta\mu = eV$ is the chemical potential difference due to the bias voltage V, $G_0 = 2e^2/h$ is the quantum of conductance. The current and the power noise may include contributions from multiple channels, with $\tau_{0,i}$ the transmission probability of the ith channel evaluated at the Fermi energy μ. Eq. (S5) is well known; we retrieve it in Sec. S3 as a special limit of a more general expression.

Low bias measurements of shot noise in atomic-scale and molecular junctions agree well with Eq. (S5), see for example Refs.[3–6] Specifically, when the temperature is low relative to the bias, $\coth(\frac{|\Delta\mu|}{2k_BT}) \to 1$, and we get

$$S_{\Delta\mu}^{T\to 0} = 2|\Delta\mu|GF. \tag{S6}$$

Here, $F = \sum_i \tau_i(1-\tau_{0,i})/\sum_i \tau_{0,i}$ is the Fano factor, $G = G_0 \sum_i \tau_{0,i}$ stands for the electrical conductance. The noise (S6) is linear in voltage. Therefore, nonlinearity of the shot noise at high voltage corresponds to an 'anomalous' behavior. Since $\langle I\rangle = GV$ and $\Delta\mu = eV$, we can organize Eq. (S6) in its familiar form as $S_{\Delta\mu}^{T\to 0} = 2e|\langle I\rangle|F$.

We now consider a junction at equilibrium, $\Delta\mu = 0$. Eq. (S2) then reduces to the Johnson-Nyquist thermal noise,

$$S_{\Delta\mu=0}^{T} = 4k_BTG, \tag{S7}$$

with the electrical conductance $G = \frac{2e^2}{h}\int d\epsilon\tau(\epsilon)\left(-\frac{df}{d\epsilon}\right)$. Note that we can also approach the equilibrium limit from Eq. (S5) and arrive at a corresponding result. Nevertheless, Eq. (S7) holds without assuming a constant transmission function.

S3 Derivation of Eqs. (3)-(8): anomalous shot noise

We begin with the calculation of the current (S1) using the transmission function (S3), and the chemical potential (S4),

$$\begin{aligned} I &= \frac{2e}{h}\int_{-\infty}^{\infty} d\epsilon \left[f(\epsilon,\mu_L,T)-f(\epsilon,\mu_R,T)\right]\left[\tau_0+\tau'(\mu)(\epsilon-\mu)\right] \\ &= \frac{2e}{h}\tau_0\Delta\mu+\frac{2e}{h}\tau'(\mu)\int_{-\infty}^{\infty} d\epsilon \left[f(\epsilon,\mu_L,T)-f(\epsilon,\mu_R,T)\right]\frac{1}{2}\left[\epsilon-\mu_L+\epsilon-\mu_R+\Delta\mu(2\alpha-1)\right] \\ &= \frac{2e}{h}\left[\tau_0\Delta\mu+\tau'(\mu)(\Delta\mu)^2\left(\alpha-\frac{1}{2}\right)\right], \end{aligned}$$

where we used the relation $\mu=(\mu_L+\mu_R)/2+\Delta\mu\left(\frac{1}{2}-\alpha\right)$.

We examine next the behavior of shot noise under high voltage; we assume that there is no applied temperature difference. We begin by evaluating S_1 in Eq. (S2) using the linear expansion for the transmission function, Eq. (S3). For convenience, we assume a single channel. We omit the prefactor $\frac{4e^2}{h}$ and re-install it only at the end of our derivation,

$$S_1 = \int_{-\infty}^{\infty} d\epsilon \left(-k_BT\frac{\partial f_L}{\partial\epsilon}-k_BT\frac{\partial f_R}{\partial\epsilon}\right)\times\left[\tau_0+\tau'(\mu)(\epsilon-\mu)\right]^2. \tag{S8}$$

Here, $f_\nu=f(\epsilon,\mu_\nu,T)$, $\Delta\mu=\mu_L-\mu_R$, $\mu_L=\mu+\alpha\Delta\mu$, $\mu_R=\mu-(1-\alpha)\Delta\mu$ and $T=T_L=T_R$. Explicitly,

$$\begin{aligned} S_1 &= \int_{-\infty}^{\infty} d\epsilon\Bigg\{(-k_BT)\left[\tau_0^2\frac{\partial f_L}{\partial\epsilon}+2\tau_0\tau'(\mu)(\epsilon-\mu)\frac{\partial f_L}{\partial\epsilon}+[\tau'(\mu)]^2(\epsilon-\mu)^2\frac{\partial f_L}{\partial\epsilon}\right] \\ &+ (-k_BT)\left[\tau_0^2\frac{\partial f_R}{\partial\epsilon}+2\tau_0\tau'(\mu)(\epsilon-\mu)\frac{\partial f_R}{\partial\epsilon}+[\tau'(\mu)]^2(\epsilon-\mu)^2\frac{\partial f_R}{\partial\epsilon}\right]\Bigg\}. \end{aligned} \tag{S9}$$

We now evaluate the different terms,

$$\begin{aligned}
I_1 &\equiv \int_{-\infty}^{\infty} d\epsilon(-k_BT)\tau_0^2\frac{\partial f_L}{\partial\epsilon} = k_BT\tau_0^2, \\
I_2 &\equiv \int_{-\infty}^{\infty} d\epsilon(-k_BT)2\tau_0\tau'(\mu)\left[\epsilon-(\mu_L-\alpha\Delta\mu)\right]\frac{\partial f_L}{\partial\epsilon} \\
&= \int_{-\infty}^{\infty} d\epsilon(-k_BT)2\tau_0\tau'(\mu)(\epsilon-\mu_L)\frac{\partial f_L}{\partial\epsilon} + \int_{-\infty}^{\infty} d\epsilon(-k_BT)2\tau_0\tau'(\mu)\alpha\Delta\mu\frac{\partial f_L}{\partial\epsilon} \\
&= 2k_BT\tau_0\tau'(\mu)\alpha\Delta\mu, \\
I_3 &\equiv \int_{-\infty}^{\infty} d\epsilon(-k_BT)[\tau'(\mu)]^2\left[\epsilon-(\mu_L-\alpha\Delta\mu)\right]^2\frac{\partial f_L}{\partial\epsilon} \\
&= \int_{-\infty}^{\infty} d\epsilon(-k_BT)[\tau'(\mu)]^2\left[(\epsilon-\mu_L)^2+2\alpha\Delta\mu(\epsilon-\mu_L)+\alpha^2(\Delta\mu)^2\right]\frac{\partial f_L}{\partial\epsilon} \\
&= k_BT[\tau'(\mu)]^2\frac{\pi^2k_B^2T^2}{3} + k_BT[\tau'(\mu)]^2\alpha^2(\Delta\mu)^2. \qquad \text{(S10)}
\end{aligned}$$

Summing up these integrals, along with the corresponding contributions from the right side, we get

$$\begin{aligned}
S_1 &= 2k_BT\tau_0^2 + 2k_BT\tau_0\tau'(\mu)\Delta\mu\alpha - 2k_BT\tau_0\tau'(\mu)\Delta\mu(1-\alpha) \\
&+ 2k_BT[\tau'(\mu)]^2\frac{\pi^2k_B^2T^2}{3} + k_BT[\tau'(\mu)]^2\left[\alpha^2(\Delta\mu)^2+(1-\alpha)^2(\Delta\mu)^2\right]. \qquad \text{(S11)}
\end{aligned}$$

Next, we evaluate S_2 in Eq. (S2). Under bias voltage it can be organized as

$$S_2 = \coth\left(\frac{\Delta\mu}{2k_BT}\right)\int_{-\infty}^{\infty} d\epsilon\left[f_L(\epsilon)-f_R(\epsilon)\right]\left[\tau_0+\tau'(\mu)(\epsilon-\mu)\right]\left[1-\tau_0-\tau'(\mu)(\epsilon-\mu)\right]. \qquad \text{(S12)}$$

The integral can be evaluated *exactly* using the following relations,

$$
\begin{aligned}
I_4 &\equiv \coth\left(\frac{\Delta\mu}{2k_BT}\right)\int_{-\infty}^{\infty} d\epsilon[f_L(\epsilon)-f_R(\epsilon)]\tau_0(1-\tau_0) = \tau_0(1-\tau_0)\Delta\mu\coth\left(\frac{\Delta\mu}{2k_BT}\right), \\
I_5 &\equiv \coth\left(\frac{\Delta\mu}{2k_BT}\right)\int_{-\infty}^{\infty} d\epsilon[f_L(\epsilon)-f_R(\epsilon)](1-2\tau_0)\tau'(\mu)(\epsilon-\mu) \\
&= \coth\left(\frac{\Delta\mu}{2k_BT}\right)(1-2\tau_0)\tau'(\mu)\int_{-\infty}^{\infty} d\epsilon[f_L(\epsilon)-f_R(\epsilon)]\left\{\left[\epsilon-\left(\mu+\left(\alpha-\frac{1}{2}\right)\Delta\mu\right)\right]+\left(\alpha-\frac{1}{2}\right)\Delta\mu\right\} \\
&= \coth\left(\frac{\Delta\mu}{2k_BT}\right)(1-2\tau_0)\tau'(\mu)\left[\alpha-\frac{1}{2}\right](\Delta\mu)^2, \\
I_6 &\equiv \coth\left(\frac{\Delta\mu}{2k_BT}\right)\int_{-\infty}^{\infty} d\epsilon[f_L(\epsilon)-f_R(\epsilon)][\tau'(\mu)]^2\left\{\left[\epsilon-\left(\mu+\left(\alpha-\frac{1}{2}\right)\Delta\mu\right)\right]+\left(\alpha-\frac{1}{2}\right)\Delta\mu\right\}^2 \\
&= \coth\left(\frac{\Delta\mu}{2k_BT}\right)[\tau'(\mu)]^2\left[\Delta\mu\frac{\pi^2k_B^2T^2}{3}+\frac{1}{12}(\Delta\mu)^3+\left(\alpha-\frac{1}{2}\right)^2(\Delta\mu)^3\right]. \qquad \text{(S13)}
\end{aligned}
$$

Overall, we get

$$
\begin{aligned}
S_2 &= \tau_0(1-\tau_0)\Delta\mu\coth\left(\frac{\Delta\mu}{2k_BT}\right)+\coth\left(\frac{\Delta\mu}{2k_BT}\right)(1-2\tau_0)\tau'(\mu)\left(\alpha-\frac{1}{2}\right)(\Delta\mu)^2 \\
&- \coth\left(\frac{\Delta\mu}{2k_BT}\right)[\tau'(\mu)]^2\left[\Delta\mu\frac{\pi^2k_B^2T^2}{3}+\frac{1}{12}(\Delta\mu)^3+\left(\alpha-\frac{1}{2}\right)^2(\Delta\mu)^3\right]. \qquad \text{(S14)}
\end{aligned}
$$

Combining S_1 [Eq. (S11)] and S_2, we get the voltage-activated anomalous shot noise,

$$
\begin{aligned}
S^T_{\Delta\mu} &= 2k_BT\tau_0^2+2k_BT\tau_0\tau'(\mu)\Delta\mu\alpha-2k_BT\tau_0\tau'(\mu)\Delta\mu(1-\alpha) \\
&+ 2k_BT[\tau'(\mu)]^2\frac{\pi^2k_B^2T^2}{3}+k_BT[\tau'(\mu)]^2\left[\alpha^2(\Delta\mu)^2+(1-\alpha)^2(\Delta\mu)^2\right] \\
&+ \tau_0(1-\tau_0)\Delta\mu\coth\left(\frac{\Delta\mu}{2k_BT}\right)+\coth\left(\frac{\Delta\mu}{2k_BT}\right)(1-2\tau_0)\tau'(\mu)\left(\alpha-\frac{1}{2}\right)(\Delta\mu)^2 \\
&- \coth\left(\frac{\Delta\mu}{2k_BT}\right)[\tau'(\mu)]^2\left[\Delta\mu\frac{\pi^2k_B^2T^2}{3}+\frac{1}{12}(\Delta\mu)^3+\left(\alpha-\frac{1}{2}\right)^2(\Delta\mu)^3\right]. \qquad \text{(S15)}
\end{aligned}
$$

Multiplying it by $2G_0 = \dfrac{4e^2}{h}$ we obtain Eqs. (4)-(6) in the main text. It is significant to note that this result is exact in $\Delta\mu$, to the order of $\tau'(\mu)$ considered.

S4 Theory-experiment analysis of other types of junctions

So far, our focus has been on junctions whose transmission function can be approximated by the expansion (S3) around the Fermi energy. This expansion leads to a differential conductance that is linear in voltage. In this section, we consider an alternative form for the transmission function, relevant for a complementary class of junctions,

$$\tau(\epsilon) \approx \tau_0 + \frac{1}{2}\tau''(\mu)(\epsilon-\mu)^2. \tag{S16}$$

We again allow the voltage bias to drop asymmetrically around the equilibrium Fermi energy, $\mu_L = \mu + \alpha\Delta\mu$, $\mu_R = \mu - (1-\alpha)\Delta\mu$, with $0 \leq \alpha \leq 1$. Using the Landauer formula we obtain the averaged charge current as,

$$\langle I\rangle = \frac{2e}{h}\tau_0\Delta\mu + \frac{e}{h}\tau''(\mu)\left[\Delta\mu\frac{\pi^2 k_B^2 T^2}{3} + \frac{1}{12}(\Delta\mu)^3 + \left(\alpha-\frac{1}{2}\right)^2(\Delta\mu)^3\right]. \tag{S17}$$

We now assume that the temperature is low relative to the bias voltage and derive the differential conductance,

$$\frac{d\langle I\rangle}{dV}\Big|_{T\to 0} = G_0\tau_0 + \frac{3G_0}{2}\tau''(\mu)\left[\frac{1}{12} + \left(\alpha-\frac{1}{2}\right)^2\right](\Delta\mu)^2. \tag{S18}$$

By fitting the differential conductance to a parabola we obtain the curvature $B \equiv \frac{3}{2}G_0\tau''(\mu)[1/12 + (\alpha-1/2)^2]$, with $\frac{d\langle I\rangle}{dV}|_{T\to 0} = G_0\tau_0 + B(\Delta\mu)^2$. Note that the quadratic term in $\frac{d\langle I\rangle}{dV}$ is sustained even when $\alpha = 1/2$.

Repeating the procedure of Sec. S3, we derive a closed form formula for the current noise

using the transmission function (S16). Here, we present only the low temperature limit,

$$\begin{aligned} S_{\Delta\mu}^{T\to 0} &= 4G_0 k_B T \tau_0^2 + 2G_0\tau_0(1-\tau_0)\Delta\mu \coth\left(\frac{\Delta\mu}{2k_BT}\right) \\ &+ 2G_0(1-2\tau_0)\frac{\tau''(\mu)}{2}\left[\frac{1}{12}+\left(\alpha-\frac{1}{2}\right)^2\right]|(\Delta\mu)|^3 \end{aligned} \tag{S19}$$

It is significant to note that the curvature B, which determines the nonlinearity of the differential conductance, dictates the anomalous component of the shot noise. Nevertheless, in the present model, Eq. (S16), we cannot in practice determine the extent of bias asymmetry α.

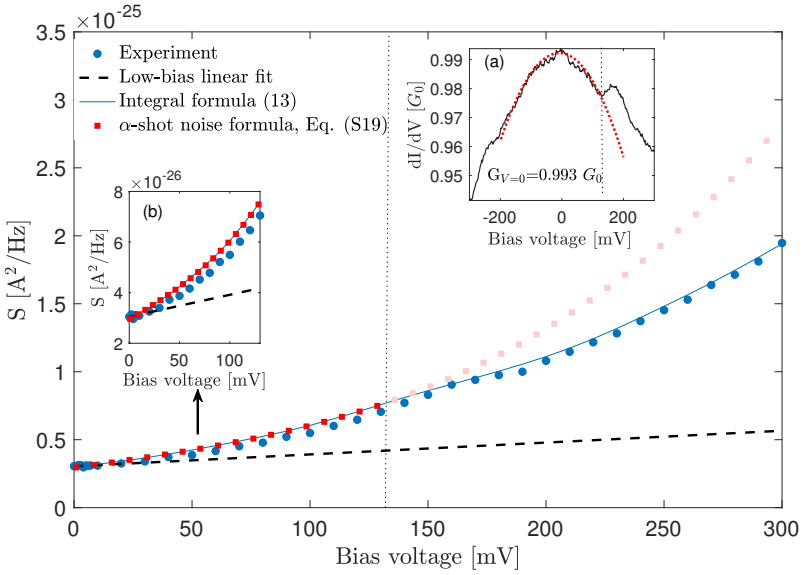

Figure S1: Anomalous shot noise with a quadratic differential conductance-voltage characteristics. Measurements (○) are compared to a linear fit at low voltage (dashed) and to the anomalous shot noise formula Eq. (S19) (□) using $T = 7$ K, $\tau_{0,1}$=0.99, $\tau_{0,2}$=0.00. We further show (full) simulations based on Eq. (13). (a) We fit the differential conductance data (full) to a parabola (dotted) within the region -200 to 120 mV and get the curvature $B = -0.826\ G_0/(eV)^2$, which is substituted into Eq. (S19) to reproduce the nonlinear shot noise (b), showing an excellent agreement. Results from the nomalous shot noise formula outside the proper fitting window are further displayed in the main plot (light □).

We illustrate the analysis and the validity of Eq. (S19) on experimental data of shot noise in Au atomic junctions. Besides results in the main text, Figure S1 displays data for which the differential conductance is approximately quadratic around zero voltage (inset), which

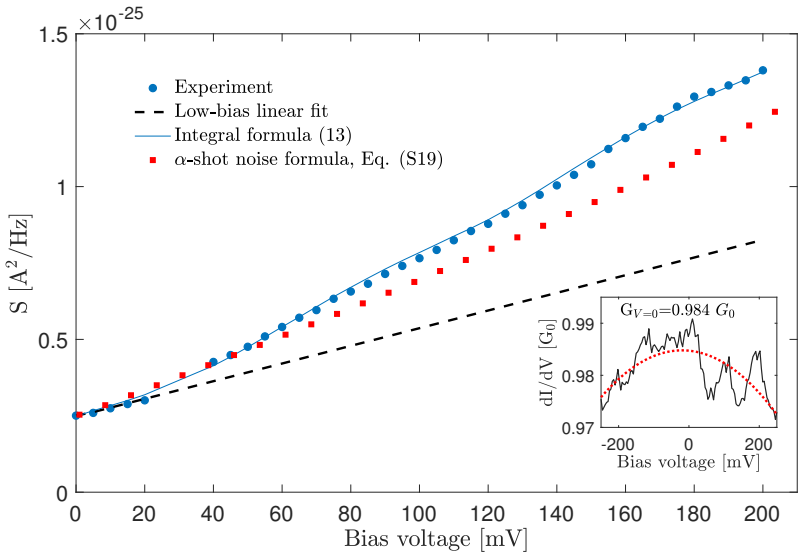

Figure S2: Anomalous shot noise with a possible quadratic differential conductance-voltage characteristics. Measurements (○) are compared to the anomalous shot noise formula Eq. (S19) (□) using $T = 6$ K, $\tau_{0,1}$=0.984, $\tau_{0,2}$=0.0018. We further show (full) simulations based on Eq. (13). Inset: We fit the differential conductance (full) to a parabola (dotted) and get the curvature $B = -0.169$ $G_0/(eV)^2$, which is substituted into Eq. (S19) to reproduce the nonlinear shot noise.

make it suitable for the present analysis. Following our procedure, we extract the curvature of the parabola B from the differential conductance and employ it in Eq. (S19) to generate the current noise. In Fig. 7 (main text), the quadratic behavior of the differential conductance with voltage extends up to 200 mV, and the noise is indeed well reproduced throughout the whole range. In contrast, in Fig. S1, the quadratic behavior only extends up to 120 mV, beyond which deviations show; in accordance, we properly capture the experimental data for the shot noise up to this voltage. Remarkably, in Fig. S1 the nonlinear (cubic) term almost immediately dominates at low voltage, since the curvature is quite large. Finally, Fig. S2 displays differential conductance data that does not show a definite quadratic trend (extending the experiment to higher voltage could strengthen this model). Nevertheless, we test the quadratic formula on this data and show that we qualitatively capture the overall trend of the experimental shot noise, observing an enhancement of noise relative to the low bias case.

S5 Experimental procedure

Formation of Au atomic Junctions. The mechanically controllable break junction technique[7] in cryogenic temperature is used to form Au atomic junctions. A gold wire (99.99%, 0.1 mm diameter, Goodfellow), with a partial cut in its center is attached to a flexible and insulating substrate. This structure is placed in a vacuum chamber, pumped to 10^{-5} mbar and cooled to 4.2 K. The sample is then bent by a piezoelectric element. As a result, the wire is stretched and gradually thinned until a contact with only few atoms down to a single atom in its cross-section is formed between the two wire segments. To measure conductance and noise across the formed atomic junction, the two wire segments are used as electrodes. Repeated squeezing of the electrodes against each other, followed by stretching the reformed contact is used to obtain new atomic junctions. This procedure allows the characterization of an ensemble of atomic junctions with different structures.

Differential Conductance Measurements. Differential conductance vs. voltage measurements ($d\langle I\rangle/dV$ vs. V) are conducted via a standard lock-in technique, using a Stanford Research SR830 lock-in amplifier. A DC bias voltage signal from a National Instruments (NI) PCI-6221 DAQ card is modulated by an AC voltage produced by the lock-in amplifier (1 mV rms at about 3.33 kHz). The resulting current across the sample is amplified by a current preamplifier (SR570) and sent back to the lock-in to extract the corresponding signal at the frequency of the applied AC modulation. Differential conductance measurements are performed before and after each set of noise measurements in order to verify that the contact maintained its stability during the noise measurement by comparing the two differential conductance spectra.

Shot Noise Measurements. Noise measurements are performed on the atomic junctions using a dedicated circuit.[8] To measure noise on atomic junctions, the sample is disconnected from the conductance measurement circuit and connected to the dedicated circuit using switches. The sample is current-biased by a Yokogawa GS200 SC voltage source connected to the sample through two 0.5MΩ resistors located in proximity to the sample. The

resulting voltage noise is amplified by a custom-made differential low-noise amplifier and analyzed via a NI PXI-5922 DAQ card, using a LabView implemented fast Fourier transform analysis. For each stable atomic junction, noise measurements are conducted at a set of different bias currents, where at each bias 3,000 measurements of noise spectra are taken and averaged.

S6 Estimation of the contribution of the $1/f$ noise

At high voltage, other noise sources could contribute to the anomalous behavior. Specifically, the $1/f$ noise grows quadratically with voltage, and its contribution could become significant. As representative examples, in Figs S3 and S4 we display the power spectra of the noise corresponding to Figs. 4 and 6 in the main text. At low frequency, the power spectra shows the $1/f$ noise. The white noise component, which comprises the thermal noise and shot noise is taken in the region $f \approx 1 \times 10^5$ Hz.

We assess the contribution of the $1/f$ component in an approximate manner as follows. First, at each applied voltage we subtract the mean white noise value, to identify the 'pure' $1/f$ contribution. Next, plotting this data on a log-log scale, we extract the power α, $S(f) = S_c/f^\alpha$, with S_c a prefactor, which depends on the applied voltage.

Performing this analysis on the data presented in Fig. S3, we obtain the exponent, which somewhat varies with voltage, $\alpha = 1.5 - 1.7$. Since we are interested in the contribution of $1/f$ noise at high voltage, we use $\alpha = 1.66$ at 200 mV. To extract S_c at 200 mV we focus on the low frequency region, and use e.g. the measured value of $S(f = 5000 \text{ Hz}) = 2.3 \times 10^{-17}$ V^2/Hz and the calculated power $\alpha = 1.66$. This results in $S_c \sim 3.2 \times 10^{-11}$ V^2/Hz. We can now estimate the contribution of the $1/f$ noise at higher frequencies, in what we identify as

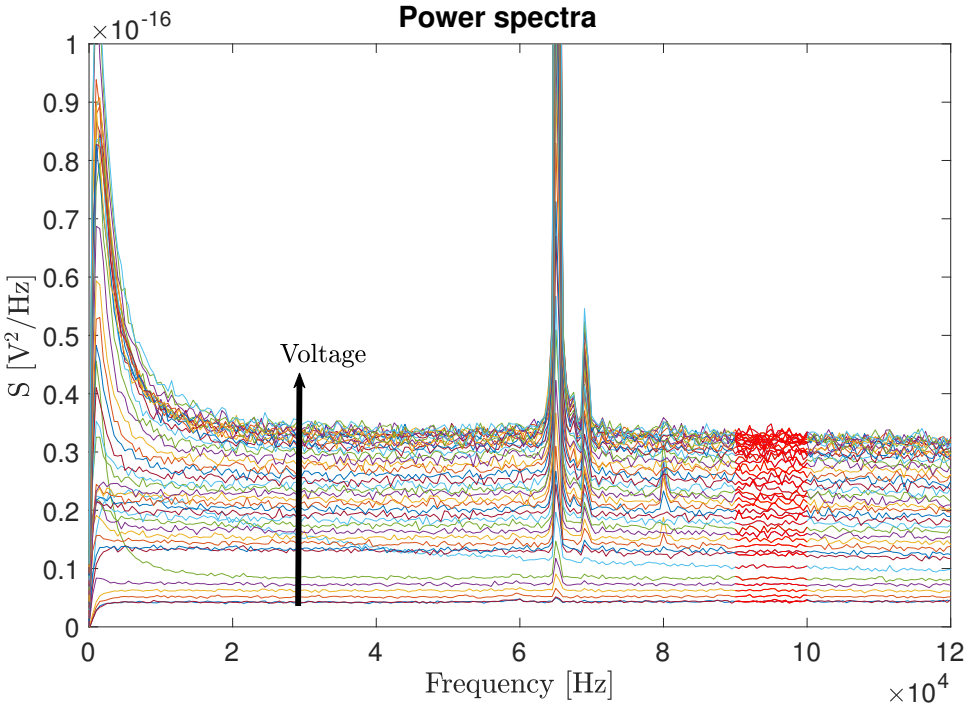

Figure S3: Power spectra for different applied voltage. The red region marks the portion of the noise used in the shot noise analysis, leading to Fig. 4 in the main text.

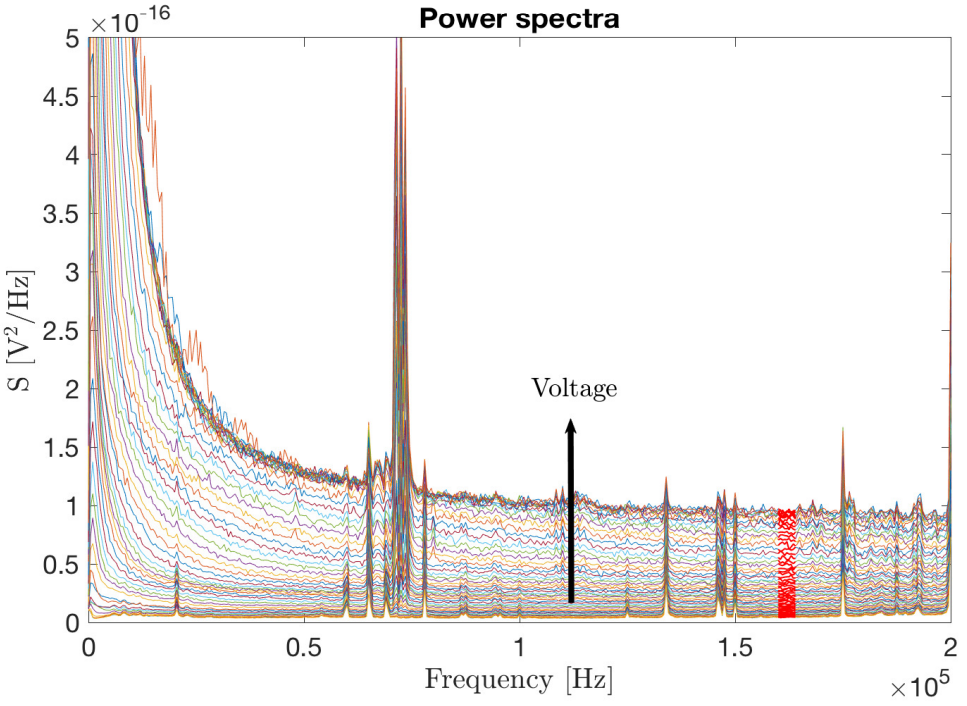

Figure S4: Power spectra for different applied voltage. The red region marks the portion of the noise used in the shot noise analysis, leading to Fig. 6 in the main text.

white noise, say at $f = 9 \times 10^4$ Hz,

$$\begin{aligned} S(f) &= S_c/f^\alpha \\ &= 3.2 \times 10^{-11} \times G^2 \times (9 \times 10^4)^{-1.66} = 1.03 \times 10^{-27} \mathrm{A}^2/\mathrm{Hz}, \end{aligned} \tag{S20}$$

where we used $G = 0.95\ G_0$. The anomalous noise presented in Fig. 4 reaches 2×10^{-25} A^2/Hz at high voltage, and we conclude that the $1/f$ noise contributes less than 1% to this value.

A similar analysis is performed on the power spectra in Fig. S4, which corresponds to Fig. 6 in the main text. Here, at 240 mV we obtain the power $\alpha \sim 1.7$ and the coefficient $S_c = 2.66 \times 10^{-9}$ V^2/Hz, which leads to the residual $1/f$ noise $S(f = 1.6 \times 10^5$ Hz)$\sim$ 2.08×10^{-26} A^2/Hz, using G=0.96 G_0. In contrast to the former example where the $1/f$ noise is negligible, here we estimate that the $1/f$ noise contributes $\sim$10% to the noise at high voltage, beyond 200 mV. However, in all other cases we confirmed that the $1/f$ noise level was minor, less than 3%, and that the anomalous noise examined was indeed white with negligible frequency-dependent contributions.

References

1. Blanter, Ya. M.; Buttiker, M. Shot Noise in Mesoscopic Conductors. Phys. Rep. **2000,** *336*, 1.

2. Lesovik, G. B. Excess Quantum Shot Noise in 2D Ballistic Point Contacts. JETP Lett. **1989**, *49*, 592.

3. Djukic, D.; van Ruitenbeek, J. M. Shot Noise Measurements on a Single Molecule. Nano Lett. **2006**, *6*, 789-793.

4. Chen, R.; Matt, M.; Pauly, F.; Cuevas, J. C.; Natelson, D. Shot Noise Variation within

Ensembles of Gold Atomic Break Junctions at Room Temperature. J. Phys. Condens. Matter. **2014**, *26*, 474204.

5. Karimi, M. A.; Bahoosh, S. G.; Herz, M.; Hayakawa, R.; Pauly, F.; Scheer, E. Shot Noise of 1,4-Benzenedithiol Single-Molecule Junctions. Nano Lett. **2016**, *16*, 1803.

6. Vardimon, R.; Klionsky, M.; Tal, O. Experimental Determination of Conduction Channels in Atomic-Scale Conductors Based on Shot Noise Measurements. Phys. Rev. B **2013**, *88*, 161404 R.

7. Muller, C. J.; van Ruitenbeek, J. M.; de Jongh, L. J. Experimental Observation of the Transition From Weak Link to Tunnel Junction. Phys. C Supercond. its Appl. **1992**, *191*, 485-504.

8. Shein-Lumbroso, O.; Simine, L.; Nitzan, A.; Segal, D.; Tal, O. Electronic Noise due to Temperature Difference in Atomic-Scale Junctions. Nature **2018**, *562*, 240-244.